Exciton Fine Structure in InAs Quantum Dots with Cavity-Enhanced Emission at Telecommunication Wavelength and Grown on a GaAs(111)*A* Vicinal Substrate

A. Barbiero,[1,2,*,‡] A. Tuktamyshev,[3,4,†,‡] G. Pirard,[5] J. Huwer,[1] T. Müller,[1] R.M. Stevenson,[1] S. Bietti,[3] S. Vichi,[3,4] A. Fedorov,[6] G. Bester,[5] S. Sanguinetti,[3,6] and A.J. Shields[1]

[1] *Toshiba Europe Limited, 208 Cambridge Science Park, Cambridge CB4 0GZ, United Kingdom*
[2] *Department of Physics and Astronomy, University of Sheffield, Hounsfield Road, Sheffield S3 7RH, United Kingdom*
[3] *Laboratory for Nanostructure Epitaxy and Spintronics on Silicon (L-NESS) and Material Science Department, Università degli Studi di Milano Bicocca, via R. Cozzi 55, Milano 20125, Italy*
[4] *INFN—Sezione di Milano Bicocca, Piazza della Scienza 3, Milano, Italy*
[5] *Physical Chemistry and Physics Departments, University of Hamburg, Luruper Chaussee 149, Hamburg, Germany*
[6] *Laboratory for Nanostructure Epitaxy and Spintronics on Silicon (L-NESS) and National Research Council (CNR)—Institute for Photonics and Nanotechnologies (IFN), Piazza Leonardo da Vinci 32, Milano, Italy*

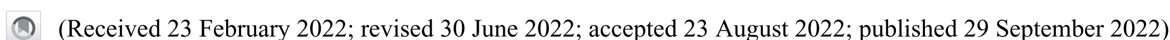
(Received 23 February 2022; revised 30 June 2022; accepted 23 August 2022; published 29 September 2022)

The efficient generation of entangled photons at telecom wavelength is essential for the success of many quantum communication protocols and the development of fiber-based quantum networks. Entangled light can be generated by solid-state quantum emitters with naturally low fine-structure splitting, such as highly symmetric InAs quantum dots (QDs) grown on (111)-oriented surfaces. The incorporation of these QDs into optical cavities is crucial to achieve sufficient signal intensities for applications but has so far shown major complications. In this work, we present droplet epitaxy of telecom-wavelength InAs QDs within an optical cavity on a vicinal (2° miscut) GaAs(111)*A* substrate. We show a remarkable enhancement of the photon extraction efficiency compared to previous reports together with a reduction of the density that facilitates the isolation of single spectral lines. Moreover, we characterize the exciton-fine-structure splitting and employ numerical simulations under the framework of the empirical-pseudopotential and configuration-interaction methods to study the impact of the miscut on the optical properties of the QDs. We demonstrate that the presence of the miscut steps influences the polarization of the neutral excitons and introduces a preferential orientation in the C_{3v} symmetry of the surface.

DOI: 10.1103/PhysRevApplied.18.034081

I. INTRODUCTION

Single and entangled photon emitters are fundamental building blocks for emerging technologies such as quantum communication protocols and quantum networks [1,2]. In this framework, sources of entangled photon pairs based on the biexciton (XX)−exciton (X) recombination cascade in semiconductor quantum dots (QDs) [3–5] offer multiple advantages such as electrical control, tunability, and integration with various photonic structures [6–12]. However, QDs typically show a fine-structure splitting (FSS) between the exciton eigenstates larger than the linewidth of the transition [13,14], which is caused by anisotropies in their shape or composition and complicates entanglement-based experiments.

One solution for the development of highly symmetric QDs with low FSS is to self-assemble them on (111)-oriented substrates due to the natural C_{3v} symmetry of the surface [15–17]. Moreover, for long-distance quantum communication and integration with the existing fiber infrastructure, it is necessary to select a platform that provides emission at telecom wavelength, such as InAs/GaAs QDs [18]. It is worth noting that InAs QDs cannot be grown on GaAs(111)*A* using the common Stranski-Krastanov (SK) method. In fact, InAs heteroepitaxy on GaAs(111)*A* proceeds with the formation of misfit dislocation at the InAs-GaAs interface, resulting in an effective strain relaxation without nucleation of three-dimensional islands [19]. Instead, they require the more advanced droplet-epitaxy (DE) technique [20,21], which relies on the formation of group-III metal droplets followed by crystallization in a group-V atmosphere. DE offers better control over the QD self-assembly dynamics and guarantees fine tuning of the shape, size, and density

*andrea.barbiero@crl.toshiba.co.uk
†artur.tuktamyshev@unimib.it
‡These authors contributed equally to this work.

 © 2022 American Physical Society

of the nanostructures [22,23]. The formation of telecom-wavelength InAs QDs on GaAs(111)*A* with a FSS as low as 16 μeV has been recently demonstrated [24]. Nevertheless, previous works on (100) substrates suggest that the incorporation of these emitters in a one-dimensional microcavity could improve the photon extraction efficiency and generate sufficient signal intensities for applications [25–27]. Unfortunately, the deposition of distributed Bragg reflectors (DBRs) on singular, i.e., on-axis, (111) substrates has proven challenging because very low growth rates below 0.03 nm/s are required to obtain flat epilayers [28].

Here, we demonstrate self-assembly of InAs DE QDs emitting in the telecom O band within a DBR microcavity grown on a vicinal (2° miscut) GaAs(111)*A* substrate. Due to the presence of the miscut, the growth rates can be increased by up to one order of magnitude (0.14–0.28 nm/s) and therefore become similar to the ones used on standard GaAs(100) [29,30]. Moreover the propensity for twin defects in the (Al,Ga)As layers, which often limits the quality of structures grown on singular (111) substrates [29], is strongly reduced. The combination of the DE technique with the growth of a DBR microcavity enables us to meet the high-brightness and low-density criteria necessary for the spectroscopic investigation of single QDs.

II. EPITAXY

The sample is grown on an undoped vicinal GaAs(111)*A* substrate with a 2° miscut along the $[\bar{1}\bar{1}2]$ direction in a solid-source molecular-beam-epitaxy (MBE) system. After a GaAs buffer, a bottom DBR with 25 repeats of $\lambda/4$ $Al_{0.5}Ga_{0.5}As$/GaAs layers is grown at 600 °C using deposition rates of 0.28 nm/s and 0.14 nm/s, respectively. Such a DBR provides high reflectivity for a wavelength range centered around 1310 nm. Next, DE InAs QDs with an approximate density of 1×10^8 cm^{-2} are formed in the middle of a $\lambda/2$ cavity consisting of 201.6 nm of $In_{0.6}Al_{0.4}As$ (grown at 470 °C with a deposition rate of 0.14 nm/s) by supplying 1 ML (monolayer) of In at 370 °C with a deposition rate of 0.003 nm/s and then crystallizing for 8 min in an As_4 atmosphere at 300 °C. During the In deposition, the residual As_4 beam-equivalent pressure (BEP) is kept below 3×10^{-9} Torr. The As_4 valve is then opened for crystallization, resulting in a BEP of 3×10^{-5} Torr. These parameters are similar to those previously developed for growth on singular GaAs(111) substrates [18]. Finally, three $\lambda/4$ layers (GaAs/$Al_{0.5}Ga_{0.5}As$/GaAs) are deposited with the same conditions as used for the bottom DBR (for further details on the sample growth and morphology, see the Supplemental Material [31]). The asymmetric cavity is designed to limit the photon leakage into the substrate and direct the emission toward the collection optics.

III. OPTICAL CHARACTERIZATION

For optical characterization, the sample is mounted inside a closed-cycle cryostat at a temperature of 5 K and the QDs are excited by a cw laser at 785 nm. The emitted photons are collected using a fiber-coupled confocal microscope and sent to a spectrometer equipped with an (In, Ga)As photodiode array for analysis.

Figure 1(a) shows a wide-range reflectivity measurement taken on the sample. The dip in the spectrum confirms the presence of a cavity mode at the desired wavelength, which is fitted with a Gaussian curve centered at 1307 nm. The extracted full width at half maximum (FWHM) of 39 nm is similar to the value predicted by our simulations.

In Fig. 1(b), we report a typical O-band photoluminescence (PL) spectrum from the QDs. The inset shows an example of a PL measurement taken in the same setup on InAs/(In,Al)As QDs grown without DBR mirrors [24], confirming that the presence of the optical cavity leads to an enhancement of the signal intensity by a factor > 5. We also note an improvement in the signal-to-background ratio and an important reduction in the density of spectral lines, which makes it possible to isolate the emission pattern of single QDs. The FWHM of the spectral lines is extracted with a Gaussian fit, as shown in Fig. 1(c). The fitting of 30 different transitions reveals no correlation between the emission wavelength and the linewidths, which vary between 100 μeV and 550 μeV [Fig. 1(d)]. Those rather broad linewidths are consistent with previously reported values [24] and originate from the presence of point defects and threading dislocations in the (In,Al)As barrier layers.

To quantify the FSS, we employ the well-established half-wave plate (HWP) method [3,32]: we send the PL signal through a rotating HWP and a fixed linear polarizer (LP) mounted in the collection arm of the confocal microscope and we measure the resulting shift in energy at the spectrometer. An example of a FSS measurement is shown in Fig. 2(a), where the energy shift as a function of the HWP angle fits well with the expected sinusoidal behavior. A statistical distribution is obtained by repeating the measurement on 35 lines of unidentified species in the telecom O band: as reported in Fig. 2(b), approximately 50% of those lines show a FSS < 50 μeV, while larger values between 70 μeV and 300 μeV are recorded in the other cases. In general, these values are similar to those reported in the literature for DE QDs grown on GaAs(100) substrates [3].

The presence of emitters with large FSS may originate from unexpected anisotropy in some of the QDs examined. To gain more insight into this phenomenon, we carry out an additional investigation focusing on the orientation of the neutral excitons. First, we adjust the position of the sample in the cryostat such that it is possible to

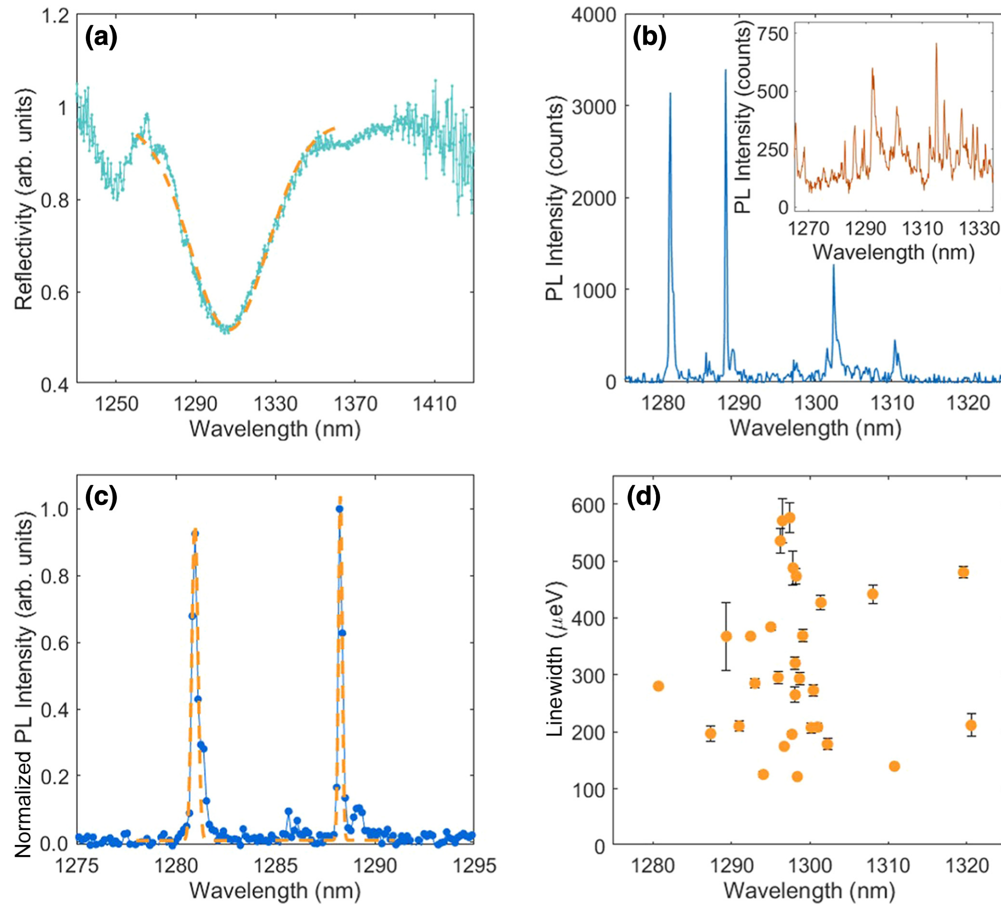

FIG. 1. (a) A reflectivity measurement taken on the optical cavity and the corresponding Gaussian fit (dashed line), showing a mode centered at 1307 nm with a full width at half maximum (FWHM) of 39 nm. (b) A typical photoluminescence (PL) spectrum of an individual InAs QD within the optical cavity under cw-laser excitation at 785 nm. The inset shows an example of a PL spectrum measured in equivalent conditions on a different sample [24] with the same InAs QDs but no distributed Bragg reflector (DBR) mirrors. (c) An exemplary Gaussian fit of two transitions from the PL spectrum reported in (b). (d) The linewidth statistics obtained by fitting 30 different spectral lines.

identify the direction of the miscut steps with respect to the laboratory frame and to the optics mounted in the collection arm of the confocal microscope. Then we repeat the FSS measurements over different QDs and select 35 neutrally charged excitons with splitting larger than 10% of the linewidth. For the majority of those emitters, we find that the oscillations of the energy offset display the first maximum for a similar HWP rotation, suggesting that the dipoles are aligned along one preferential direction [Fig. 2(c)]. No correlation between the FSS magnitude and the dipole orientation is observed.

In Fig. 2(d), we report a histogram of the dipole orientations: the Gaussian fit shows that the statistical distribution is centered around $\Delta\phi = 3.1^\circ$ ($\pm 2.2^\circ$), indicating that, for the majority of the QDs, the component of the X doublet that is higher in energy tends to be polarized along [$11\bar{2}$]. In fact, the small discrepancy of approximately 3° can easily be attributed to limited accuracy while mounting the sample. Interestingly, a small group of QDs exhibits perpendicular polarization aligned with [$1\bar{1}0$]. Since for many emitters it is not possible to identify clearly a XX-X pair and the values of FSS and $\Delta\phi$ are extracted from one spectral line only, it may be possible that those data points originate from a XX (i.e. biexcition) transition and consequently have the highest energy component of the doublet oriented at 90° with respect to the X due to conservation of energy and spin. In summary, these results suggest that the presence of a 2° miscut introduces a privileged direction in the natural C_{3v} symmetry of the system.

IV. INFLUENCE OF THE MISCUT ON THE OPTICAL PROPERTIES OF THE QDs

Following the experimental observations presented above, we carry out numerical simulations to better understand the impact of the miscut on the optical properties of the QDs (for further details on the numerical methods, see the Supplemental Material [31]). Since the entire

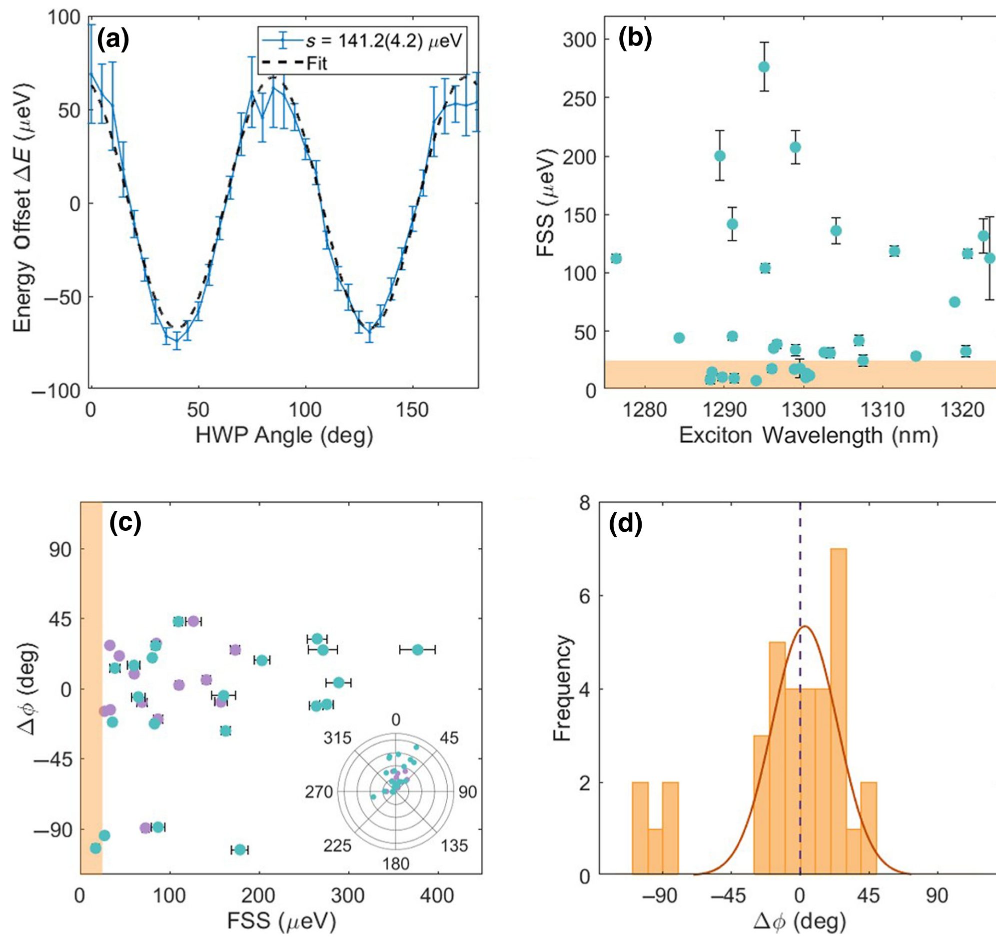

FIG. 2. (a) An example of FSS measured on an InAs QD emitting in the telecom O band using the half-wave plate (HWP) method. The dashed line is the sinusoidal fit of the energy offset. (b) The statistical distribution obtained by measuring the FSS of 35 spectral lines of unidentified species. The orange area indicates the estimated resolution limit for a transition with 250-μeV linewidth. (c) The dipole orientation of the neutral excitons as a function of the FSS measured on 35 QDs. $\Delta\phi$ is the angular offset with respect to the $[\bar{1}\bar{1}2]$ direction, while the orange area indicates the estimated resolution limit for a transition with 250-μeV linewidth. The data points are plotted in violet if it is possible to clearly identify a XX-X pair and in blue if FSS and $\Delta\phi$ are extracted from one line only. (d) The corresponding histogram with a Gaussian fit of the statistical distribution. The vertical dashed line shows the direction of the miscut steps.

structure of the sample including the (In,Al)As barrier layers and the DBR mirrors cannot be reproduced because of computational limitations, we consider three simplified material systems. First, we study GaAs/AlAs(111) QDs, which are a simple case with no strain or alloy. Then, we examine GaAs/$Al_{0.15}Ga_{0.85}As$(111) QDs to isolate the effects of alloying and, finally, InAs/GaAs(111) QDs, which are an idealized version of the sample and reveal the impact of strain due to lattice mismatch. The dots are modeled as hexagonally based truncated pyramids with 70-nm diameter, 4-nm height, and a variable miscut angle $0^\circ \leq \alpha \leq 3^\circ$ along $[\bar{1}\bar{1}2]$. They are placed in the center of a cubic simulation box filled with the barrier material and the structure is allowed to relax in order to minimize the strain energy using a generalized-valence-force-field (GVFF) model [33,34]. The single-particle Schrödinger equation is then solved (both for the conduction and valence states) under the framework of the empirical-pseudopotential method (EPM) [35] using a strained linear combination of bulk Bloch bands (SLCBBs) [36] as a basis to expand the wave functions. Then, the many-body problem is addressed through a configuration-interaction (CI) scheme [37], with the correlated exciton wave functions described as a linear combination of singly excited Slater determinants. The Hamiltonian is constructed from the electron-hole Coulomb and exchange integrals, which are calculated from the SLCBB wave functions and screened according to the Resta model [38]. In Fig. 3, we show the polarization of the two decay paths from the X state, with polar diagrams of the squared optical-transition dipole-matrix element calculated for the three cases described above as a function of the miscut

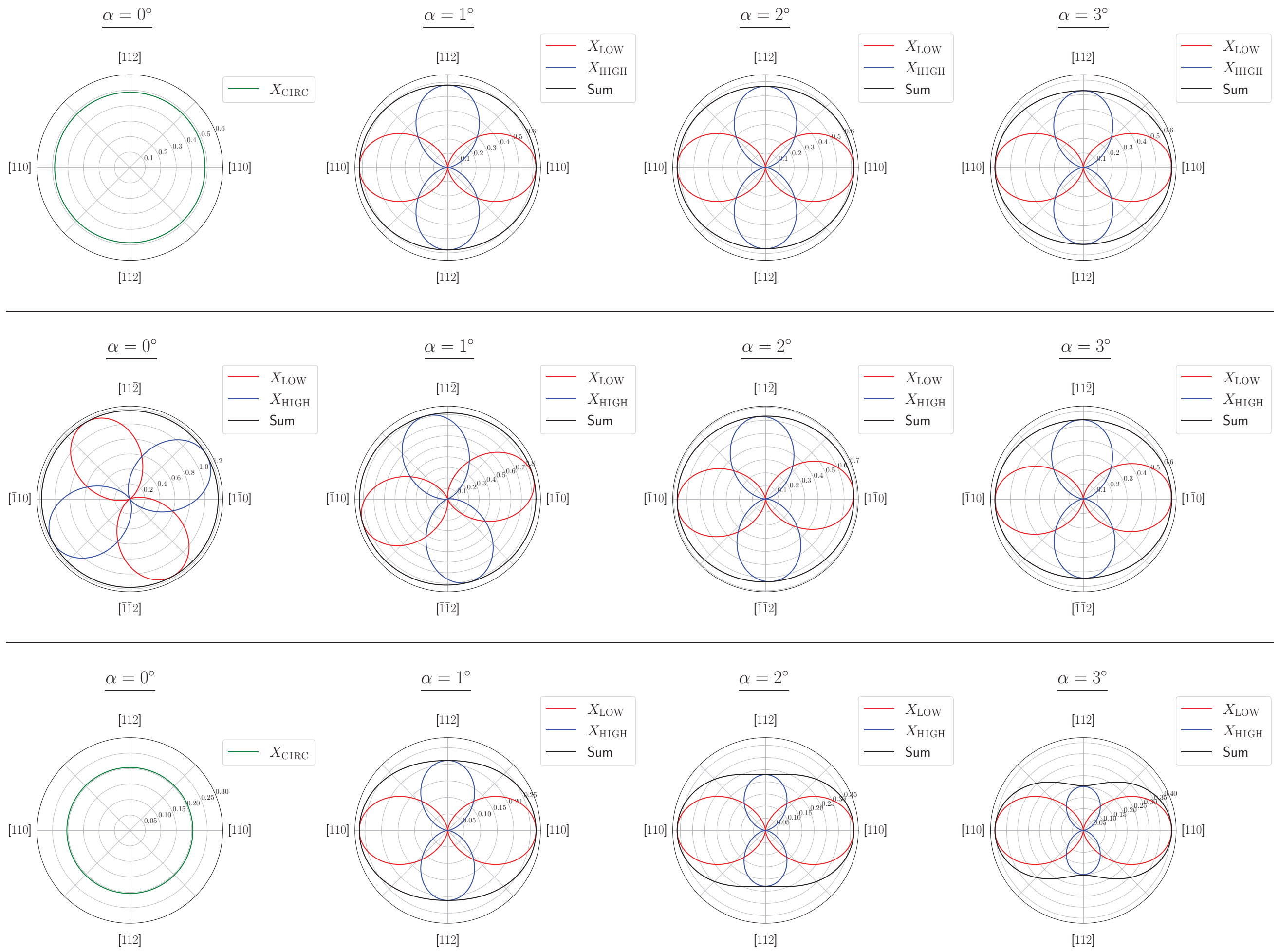

FIG. 3. Polar diagrams showing the square of the optical transition matrix element element calculated for GaAs/AlAs (top panel), $GaAs/Al_{0.15}Ga_{0.85}As$ (middle panel) and InAs/GaAs (bottom panel) QDs assuming different values of the miscut angle α. "X_{LOW}" ("X_{HIGH}") represents the lowest- (highest-) lying bright exciton state in energy, whereas two degenerate exciton bright states are labeled "X_{CIRC}". The black line labeled "Sum" represents the net total polarization from which the degree of linear polarization (DLP) is extracted.

angle α. For GaAs/AlAs(111) QDs, characterized by the perfect C_{3v} symmetry, the two decay paths from the X state are indistinguishable in the absence of miscut ($\alpha = 0°$) and can be represented by circularly polarized emission. When the miscut is introduced ($\alpha > 0°$), the two decay paths become distinguishable and the polarization of the emitted photons reconfigures such that the bright exciton state lower in energy (X_{LOW}) is polarized along the $[1\bar{1}0]$ crystal axis, whereas the bright exciton state higher in energy (X_{HIGH}) is polarized perpendicularly along $[11\bar{2}]$. The net total polarization aligns with $[1\bar{1}0]$ and the degree of linear polarization (DLP) increases slightly with the miscut angle.

If the AlAs barrier is replaced with $Al_{0.15}Ga_{0.85}As$, the degeneracy of the exciton states for $\alpha = 0°$ is broken, presumably because of the inhomogeneous composition. Furthermore, the rotation of the polarization as a function of the miscut angle is less pronounced, such that perfect alignment with the crystallographic axes is achieved for larger values of α. Finally, InAs/GaAs(111) QDs show the same behavior as GaAs/AlAs(111) QDs, but with a steeper increase of the DLP as α grows.

These simulations explain the experimental results reported in Figs. 2(c) and 2(d), confirming that the miscut is directly responsible for the appearance of a preferential orientation in all the material systems considered. We observe that the effects of alloying are weaker than the impact of the miscut, which dominates for $\alpha \geq 2°$ and is enhanced by the addition of built-in strain. These findings also support the hypothesis that the five data points in Figs. 2(c) and 2(d) with dipoles oriented along $[1\bar{1}0]$ are most likely associated with XX transitions, as explained at the end of the previous section.

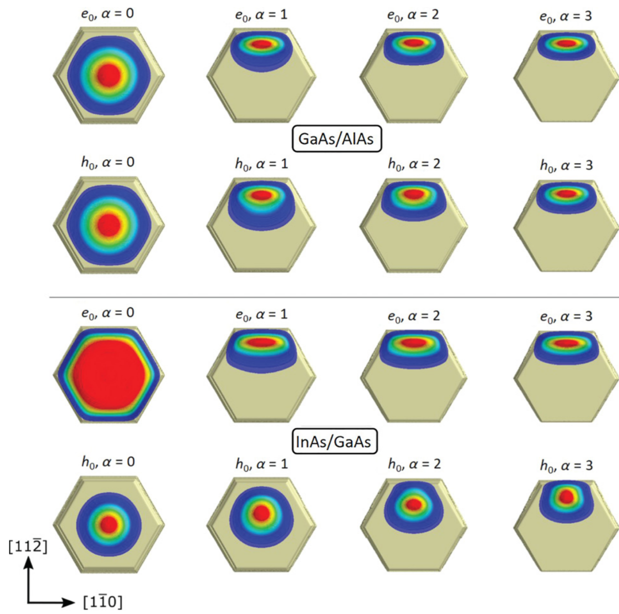

FIG. 4. The spatial profile of the electron (e_0) and hole (h_0) wave functions calculated for GaAs/AlAs QDs (top panel) and InAs/GaAs QDs (bottom panel) with miscut angle α ranging from 0° to 3°. The quantization axis, i.e., [111], is pointing toward the reader.

To clarify the physical origin of this behavior, Fig. 4 presents the charge densities of the electrons (e_0) and holes (h_0) in the conduction and valence ground states for GaAs/AlAs(111) and InAs/GaAs(111) QDs. In strain-free QDs, both the electron [Fig. 4(a)] and hole [Fig. 4(e)] wave functions exhibit a circular s-like symmetry for $\alpha = 0°$. The introduction of the miscut makes the side of the QDs toward $[11\bar{2}]$ thicker than the one toward $[\bar{1}\bar{1}2]$. As a result, the wave functions localize at the thicker edge of the dots as α grows and their spatial distribution becomes strongly elongated in the $[1\bar{1}0]$ direction. A similar progressive migration toward $[11\bar{2}]$ has been observed in the alloyed case, even though the wave functions are not characterized by a circular s-like symmetry. The picture becomes more complicated in InAs/GaAs(111) QDs: in fact, the electron wave functions can spread more than in the strain-free case and are also found to be more elongated in the $[1\bar{1}0]$ direction for $\alpha > 0°$. At the same time, the hole wave functions are more confined, so that their progressive migration toward the thicker edge of the dots as α grows is less pronounced than in GaAs/AlAs(111) QDs and their spatial spread along $[1\bar{1}0]$ is reduced. The elongation of the electron wave function increases with the miscut angle and is responsible for the growth of the intensity of polarization along $[1\bar{1}0]$ ($I^{[1\bar{1}0]}$) [39], in agreement with previous studies on elongated QDs [40].

Because of the different ability of the electron and hole wave functions to localize at the thicker edge of the InAs/GaAs(111) QDs, we observe that there may be a second source of optical anisotropy, which derives directly from the definition of dipole moment. In fact, when the miscut angle increases, the spatial separation between opposite carriers d_{eh} remains nearly constant in the $[1\bar{1}0]$ direction and diminishes along $[11\bar{2}]$, which ultimately lowers the intensity of polarization along $[11\bar{2}]$ ($I^{[11\bar{2}]}$). The combination of this effect with the elongation of the wave functions discussed above lies behind the optical anisotropy in QDs grown on (111) vicinal substrates and the resulting polarization of the neutrally charged excitons. It is now clear that in GaAs/(In,Al)As QDs, the anisotropy originates only from the elongation of the electron and hole wave functions, which are localized within the same effective volume of interaction. On the other hand, in InAs/GaAs QDs, both effects come into play, so that $I^{[11\bar{2}]}$ is modulated by the magnitude of d_{eh}. As a result, when a 2° miscut is introduced, the polarization aligns with the direction of the steps in both cases but with a different DLP.

Finally, we note that the simplified model presented in this paper is intended to provide an intuitive explanation connecting the shape of the envelope functions to the optical properties of the QDs. A rigorous treatment would require taking into account further elements such as the heavy-hole and light-hole mixing and the Bloch functions, which may affect the polarization anisotropy [41].

V. CONCLUSIONS

In this work, we incorporate DE InAs/(In,Al)As QDs grown on vicinal GaAs(111)*A* and emitting in the telecom O band into an optical microcavity based on GaAs/(Al,Ga)As DBRs. We report an enhancement of the photoluminescence signal intensities by a factor > 5 compared to similar QDs grown without DBR mirrors, together with a remarkable reduction in the density of spectral lines and background. The optical characterization of the sample also reveals that the fraction of emitters with FSS < 50 μeV is approximately 50%. Because of the wide applicability of the DE growth scheme, these results can be easily transferred to different wavelengths or material systems. Finally, we observe that the QDs tend to have dipoles aligned along a specific direction, despite the C_{3v} symmetry of the (111)-oriented substrate. In fact, numerical simulations based on the EPM and CI methods have confirmed that the presence of the miscut modifies the spatial distribution of the electron and hole wave functions, leading to their elongation in the $[1\bar{1}0]$ direction. This phenomenon influences the polarization of the excitonic states, introducing a clear preferential orientation in the natural C_{3v} symmetry of the surface, while the addition of strain due to lattice mismatch modulates and enhances this effect.

In the future, linewidths and FSS could be reduced by changing the composition of the barrier layer from

(In,Al)As to (In,Ga)As [24] and employing a smaller miscut angle, respectively. Moreover, the photon extraction efficiency could be further improved by replacing the DBR cavity with vertically emitting photonic structures, such as mesas [42], micropillars [43,44], or circular Bragg gratings [45–47], in order to create efficient quantum light sources at telecom wavelength for deployment and operation over the existing optical fiber network.

ACKNOWLEDGMENTS

This project has received partial funding from the European Union Horizon 2020 research and innovation program under the Marie Skłodowska-Curie Grant Agreement No. 721394. A. Barbiero thanks A. Tartakovskii for the academic supervision.

[1] H. J. Kimble, The quantum Internet, Nature **453**, 1023 (2008).

[2] S. Wehner, D. Elkouss, and R. Hanson, Quantum Internet: A vision for the road ahead, Science (New York) **362**, 6412 (2018).

[3] J. Skiba-Szymanska, R. M. Stevenson, C. Varnava, M. Felle, J. Huwer, T. Müller, A. J. Bennett, J. P. Lee, I. Farrer, A. B. Krysa, P. Spencer, L. E. Goff, D. A. Ritchie, J. Heffernan, and A. J. Shields, Universal Growth Scheme for Quantum Dots with Low Fine-Structure Splitting at Various Emission Wavelengths, Phys. Rev. Appl. **8**, 014013 (2017).

[4] A. Orieux, M. A. M. Versteegh, K. D. Jöns, and S. Ducci, Semiconductor devices for entangled photon pair generation: A review, Rep. Prog. Phys. **80**, 076001 (2017).

[5] D. Huber, M. Reindl, J. Aberl, A. Rastelli, and R. Trotta, Semiconductor quantum dots as an ideal source of polarization-entangled photon pairs on-demand: A review, Jpn. J. Appl. Phys. **20**, 073002 (2018).

[6] G. Kiršanskė, H. Thyrrestrup, R. S. Daveau, C. L. Dreeßen, T. Pregnolato, L. Midolo, P. Tighineanu, A. Javadi, S. Stobbe, R. Schott, A. Ludwig, A. D. Wieck, S. I. Park, J. D. Song, A. V. Kuhlmann, I. Söllner, M. C. Löbl, R. J. Warburton, and P. Lodahl, Indistinguishable and efficient single photons from a quantum dot in a planar nanobeam waveguide, Phys. Rev. B **96**, 174 (2017).

[7] R. Uppu, F. T. Pedersen, Y. Wang, C. T. Olesen, C. Papon, X. Zhou, L. Midolo, S. Scholz, A. D. Wieck, A. Ludwig, and P. Lodahl, Scalable integrated single-photon source, Sci. Adv. **6**, 50 (2020).

[8] S. E. Thomas, M. Billard, N. Coste, S. C. Wein, Priya, H. Ollivier, O. Krebs, L. Tazaïrt, A. Harouri, A. Lemaitre, I. Sagnes, C. Anton, L. Lanco, N. Somaschi, J. C. Loredo, and P. Senellart, Bright Polarized Single-Photon Source Based on a Linear Dipole, Phys. Rev. Lett. **126**, 233601 (2021).

[9] N. Tomm, A. Javadi, N. O. Antoniadis, D. Najer, M. C. Löbl, A. R. Korsch, R. Schott, S. R. Valentin, A. D. Wieck, A. Ludwig, and R. J. Warburton, A bright and fast source of coherent single photons, Nat. Nanotechnol. **16**, 399 (2021).

[10] M. Sartison, S. L. Portalupi, T. Gissibl, M. Jetter, H. Giessen, and P. Michler, Combining in-situ lithography with 3D printed solid immersion lenses for single quantum dot spectroscopy, Sci. Rep. **7**, 39916 (2017).

[11] Y. Chen, M. Zopf, R. Keil, F. Ding, and O. G. Schmidt, Highly-efficient extraction of entangled photons from quantum dots using a broadband optical antenna, Nat. Commun. **9**, 2994 (2018).

[12] A. Kaganskiy, S. Fischbach, A. Strittmatter, T. Heindel, S. Rodt, and S. Reitzenstein, Enhancing the photon-extraction efficiency of site-controlled quantum dots by deterministically fabricated microlenses, Opt. Commun. **413**, 162 (2018).

[13] D. Gammon, E. S. Snow, B. V. Shanabrook, D. S. Katzer, and D. Park, Fine Structure Splitting in the Optical Spectra of Single GaAs Quantum Dots, Phys. Rev. Lett. **76**, 3005 (1996).

[14] V. D. Kulakovskii, G. Bacher, R. Weigand, T. Kümmell, A. Forchel, E. Borovitskaya, K. Leonardi, and D. Hommel, Fine Structure of Biexciton Emission in Symmetric and Asymmetric CdSe/ZnSe Single Quantum Dots, Phys. Rev. Lett. **82**, 1780 (1999).

[15] T. Mano, M. Abbarchi, T. Kuroda, B. McSkimming, A. Ohtake, K. Mitsuishi, and K. Sakoda, Self-assembly of symmetric GaAs quantum dots on (111)A substrates: Suppression of fine-structure splitting, Appl. Phys. Express **3**, 065203 (2010).

[16] T. Kuroda, T. Mano, N. Ha, H. Nakajima, H. Kumano, B. Urbaszek, M. Jo, M. Abbarchi, Y. Sakuma, K. Sakoda, I. Suemune, X. Marie, and T. Amand, Symmetric quantum dots as efficient sources of highly entangled photons: Violation of Bell's inequality without spectral and temporal filtering, Phys. Rev. B **88**, 041306(R) (2013).

[17] F. Basso Basset, S. Bietti, M. Reindl, L. Esposito, A. Fedorov, D. Huber, A. Rastelli, E. Bonera, R. Trotta, and S. Sanguinetti, High-yield fabrication of entangled photon emitters for hybrid quantum networking using high-temperature droplet epitaxy, Nano Lett. **18**, 505 (2018).

[18] N. Ha, T. Mano, T. Kuroda, K. Mitsuishi, A. Ohtake, A. Castellano, S. Sanguinetti, T. Noda, Y. Sakuma, and K. Sakoda, Droplet epitaxy growth of telecom InAs quantum dots on metamorphic InAlAs/GaAs(111)A, Jpn. J. Appl. Phys. **54**, 04DH07 (2015).

[19] H. Yamaguchi, J. G. Belk, X. M. Zhang, J. L. Sudijono, M. R. Fahy, T. S. Jones, D. W. Pashley, and B. A. Joyce, Atomic-scale imaging of strain relaxation via misfit dislocations in highly mismatched semiconductor heteroepitaxy: InAs/GaAs(111)A, Phys. Rev., B. Condens. Matter **55**, 1337 (1997).

[20] N. Koguchi, S. Takahashi, and T. Chikyow, New MBE growth method for InSb quantum well boxes, J. Cryst. Growth. **111**, 688 (1991).

[21] M. Gurioli, Z. Wang, A. Rastelli, T. Kuroda, and S. Sanguinetti, Droplet epitaxy of semiconductor nanostructures for quantum photonic devices, Nat. Mater. **18**, 799 (2019).

[22] C. Somaschini, S. Bietti, N. Koguchi, and S. Sanguinetti, Fabrication of multiple concentric nanoring structures, Nano Lett. **9**, 3419 (2009).

[23] C. Somaschini, S. Bietti, N. Koguchi, and S. Sanguinetti, Shape control via surface reconstruction kinetics of droplet epitaxy nanostructures, Appl. Phys. Lett. **97**, 203109 (2010).

[24] A. Tuktamyshev, A. Fedorov, S. Bietti, S. Vichi, K. D. Zeuner, K. D. Jöns, D. Chrastina, S. Tsukamoto, V. Zwiller, M. Gurioli, and S. Sanguinetti, Telecom-wavelength InAs QDs with low fine structure splitting grown by droplet epitaxy on GaAs(111)A vicinal substrates, Appl. Phys. Lett. **118**, 133102 (2021).

[25] M. B. Ward, M. C. Dean, R. M. Stevenson, A. J. Bennett, D. Ellis, K. Cooper, I. Farrer, C. A. Nicoll, D. A. Ritchie, and A. J. Shields, Coherent dynamics of a telecom-wavelength entangled photon source, Nat. Commun. **5**, 3316 (2014).

[26] J. Huwer, R. M. Stevenson, J. Skiba-Szymanska, M. B. Ward, A. J. Shields, M. Felle, I. Farrer, D. A. Ritchie, and R. V. Penty, Quantum-Dot-Based Telecommunication-Wavelength Quantum Relay, Phys. Rev. Appl. **8**, 024007 (2017).

[27] T. Müller, J. Skiba-Szymanska, A. B. Krysa, J. Huwer, M. Felle, M. Anderson, R. M. Stevenson, J. Heffernan, D. A. Ritchie, and A. J. Shields, A quantum light-emitting diode for the standard telecom window around 1,550 nm, Nat. Commun. **9**, 862 (2018).

[28] L. Esposito, S. Bietti, A. Fedorov, R. Nötzel, and S. Sanguinetti, Ehrlich-Schwöbel effect on the growth dynamics of GaAs(111)A surfaces, Phys. Rev. Mater. **1**, 024602 (2017).

[29] F. Herzog, M. Bichler, G. Koblmüller, S. Prabhu-Gaunkar, W. Zhou, and M. Grayson, Optimization of AlAs/AlGaAs quantum well heterostructures on on-axis and misoriented GaAs(111)B, Appl. Phys. Lett. **100**, 192106 (2012).

[30] A. Tuktamyshev, A. Fedorov, S. Bietti, S. Tsukamoto, and S. Sanguinetti, Temperature activated dimensionality crossover in the nucleation of quantum dots by droplet epitaxy on GaAs(111)A vicinal substrates, Sci. Rep. **9**, 14520 (2019).

[31] See the Supplemental Material at http://link.aps.org/supplemental/10.1103/PhysRevApplied.18.034081 for further details on the sample growth and morphology and the numerical methods.

[32] R. J. Young, R. M. Stevenson, A. J. Shields, P. Atkinson, K. Cooper, D. A. Ritchie, K. M. Groom, A. I. Tartakovskii, and M. S. Skolnick, Inversion of exciton level splitting in quantum dots, Phys. Rev. B **72**, 113305 (2005).

[33] P. N. Keating, Effect of invariance requirements on the elastic strain energy of crystals with application to the diamond structure, Phys. Rev. **145**, 637 (1966).

[34] A. J. Williamson, L. W. Wang, and A. Zunger, Theoretical interpretation of the experimental electronic structure of lens-shaped self-assembled InAs/GaAs quantum dots, Phys. Rev., B. Condens. Matter **62**, 12963 (2000).

[35] G. Bester, Electronic excitations in nanostructures: An empirical pseudopotential based approach, J. Phys. Condens. Matter: An Institute of Physics Journal **21**, 023202 (2009).

[36] L.-W. Wang and A. Zunger, Linear combination of bulk bands method for large-scale electronic structure calculations on strained nanostructures, Phys. Rev., B. Condens. Matter **59**, 15806 (1999).

[37] A. Franceschetti, H. Fu, L. W. Wang, and A. Zunger, Many-body pseudopotential theory of excitons in InP and CdSe quantum dots, Phys. Rev., B. Condens. Matter **60**, 1819 (1999).

[38] R. Resta, Thomas-Fermi dielectric screening in semiconductors, Phys. Rev. B **16**, 2717 (1977).

[39] G. A. Narvaez, G. Bester, and A. Zunger, Excitons, biexcitons, and trions in self-assembled (In,Ga)As/GaAs quantum dots: Recombination energies, polarization, and radiative lifetimes versus dot height, Phys. Rev. B **72**, 245318 (2005).

[40] W. Sheng, Origins of optical anisotropy in artificial atoms, Appl. Phys. Lett. **89**, 173129 (2006).

[41] C. Tonin, R. Hostein, V. Voliotis, R. Grousson, A. Lemaitre, and A. Martinez, Polarization properties of excitonic qubits in single self-assembled quantum dots, Phys. Rev. B **85**, 3050 (2012).

[42] T. Gao, L. Rickert, F. Urban, J. Große, N. Srocka, S. Rodt, A. Musial, K. Zolnacz, P. Mergo, K. Dybka, W. Urbańczyk, G. Sek, S. Burger, S. Reitzenstein, and T. Heindel, A quantum key distribution testbed using a plug&play telecom-wavelength single-photon source, Appl. Phys. Rev. 011412 (2022).

[43] S. A. Blokhin, M. A. Bobrov, N. A. Maleev, J. N. Donges, L. Bremer, A. A. Blokhin, A. P. Vasil'ev, A. G. Kuzmenkov, E. S. Kolodeznyi, V. A. Shchukin, N. N. Ledentsov, S. Reitzenstein, and V. M. Ustinov, Design optimization for bright electrically-driven quantum dot single-photon sources emitting in telecom O-band, Opt. Express **29**, 6582 (2021).

[44] L. Bremer, C. Jimenez, S. Thiele, K. Weber, T. Huber, S. Rodt, A. Herkommer, S. Burger, S. Höfling, H. Giessen, and S. Reitzenstein, Numerical optimization of single-mode fiber-coupled single-photon sources based on semiconductor quantum dots, Opt. Express **30**, 15913 (2022).

[45] L. Rickert, T. Kupko, S. Rodt, S. Reitzenstein, and T. Heindel, Optimized designs for telecom-wavelength quantum light sources based on hybrid circular Bragg gratings, Opt. Express **27**, 36824 (2019).

[46] A. Barbiero, J. Huwer, J. Skiba-Szymanska, T. Müller, R. M. Stevenson, and A. J. Shields, Design study for an efficient semiconductor quantum light source operating in the telecom C-band based on an electrically-driven circular Bragg grating, Opt. Express **30**, 10919 (2022).

[47] A. Barbiero, J. Huwer, J. Skiba-Szymanska, D. J. P. Ellis, R. M. Stevenson, T. Müller, G. Shooter, L. E. Goff, D. A. Ritchie, and A. J. Shields, High-performance single-photon sources at telecom wavelength based on broadband hybrid circular Bragg gratings, ACS Photonics **9**, 3060 (2022).